

DESIGN OF A COMPACT BROADBAND ANTENNA USING CHARACTERISTIC MODE ANALYSIS FOR MICROWAVE APPLICATIONS

Ahmad Abbas Al Rimi^{1*}, Asmaa Zugari¹, Aicha Mchbal¹, Mohssine El Ouahabi²
and Mohsine Khalladi¹

(Received: 28-Dec.-2022, Revised: 1-Mar.-2023, Accepted: 20-Mar.-2023)

ABSTRACT

A compact broadband antenna of dimensions $27\text{ mm} \times 28\text{ mm} \times 1.6\text{ mm}$ and with good impedance matching is designed for high-bandwidth radio systems with a short range. To improve the impedance matching, two rectangular slots are created on the radiating element and the ground plane size is reduced to extend the ultra-wideband frequency band. The antenna bandwidth and radiation performance are analyzed using characteristic mode theory (TCM). The performance is compared to the desired specifications and the shape and size are modified to produce efficient radiation and dominant radiation patterns. The findings clearly demonstrate that the six modes are resonant with ($\lambda_n=0$). This implies that the eigenvalues of the six modes contribute strongly to dominant electromagnetic radiation and have high modal significance values around 1 at their respective frequencies. Furthermore, the characteristic angle indicates that the antenna resonates at 180° , since the six modes intersect the axis line at 180° at their respective frequencies. Experimental results show a bandwidth of 109.7% between 5.64 and 19.34 GHz, a maximum gain of 6.3 dB and a maximum efficiency of approximately 86.5%. These results make this antenna a versatile and effective choice for a wide variety of communications and electronic applications and easy to install in narrow spaces due to its easy design characteristics, small size and light weight.

KEYWORDS

Eigen currents, Eigenvalues, Characteristic modes, Satellite application, Ultra-wideband.

1. INTRODUCTION

Wireless, mobile and satellite communication technologies have developed quickly and the ability for data mobility, accessibility and the exchanging of high-quality data at high speeds between portable devices has grown incredibly quickly. In addition, as computer networks have grown in popularity, a diversity of electronic and handheld devices, as well as radio applications, have undergone a huge evolution, which continues the need to increase and enhance the bandwidth needs of measuring systems, since new specifications for measurements beyond 1 GHz are being developed for a number of standards around the world [1]. In 2002, the Federal Communications Commission (FCC) allocated a range of radio frequencies from 3.1 GHz to 10.6 GHz for unlicensed ultra-wideband (UWB) systems [2]. Since then, the practical design and implementation of a UWB system have become a challenge in academia and the telecommunications industry. The design of a UWB antenna faces challenges in terms of broadband performance, small size, radiation stability, manufacturing ease and low cost. The use of broadband antennas in systems is more practical and with the aim of enhancing antenna bandwidth, several designs have been made, including ultra-wideband antennas in the shapes of rectangles [3], patch antenna with tapered oval apertures [4], a square shape with slots serrated [5], a pyramidal horn [6], a serrated wheel [2], a rhombus-shaped [7], a triangular-shaped [8], fractal-shaped O-ring antenna [9], patch antenna grid-slotted [10], H-shaped microstrip patch antenna [11] and other shapes [12]-[13]. However, most of the relevant literature lacks a CMA analysis.

1. A. Al Rimi (Corresponding Author), A. Zugari, A. Mchbal and M. Khalladi are with Information Systems and Telecommunications Lab., Uni. of Abdelmalek Essaadi, Faculty of Science Tetuan, Morocco. Emails: alrimiahmed75@gmail.com, asmaa.zugari@gmail.com, aicha.mchbal8@gmail.com and m_khalladi@hotmail.com
2. M. El Ouahabi is with National School of Applied Sciences, Uni. of Abdelmalek Essaadi, Morocco. Email: moelouahabi@uae.ac.ma

For designing any antenna and determining the resonance in free space or analyzing the performance of an antenna, CMA is regarded as a basic approach that involves calculating the field radiated and the surface current. This theory is grounded on the MoM (Method of Moments) to solve the complete set of Maxwell's equations and evaluate the antenna performance based on eigenvalues [23]. In 1965, Garbacz suggested CMA analysis for the wire antenna. This technology was expanded for solid conducting structures by Harrington and Mautz [24]. Several more extensions of the theory were later developed by Harrington, Mautz and their students [25]-[26]. Although some researchers published their works late last century, approximately 42 years went by without the entire potential of CM being acknowledged. In 2007, the capabilities of CM were revisited by summarizing research that authors had conducted over the past several years to show that the Theory of Characteristic Modes may be utilized to execute a methodical design of various kinds of antennas [27]. Since then, interest in the theory of characteristic mode analysis has increased dramatically and the number of important articles and applications is a good indicator of the subsequent boom. Overall, characteristic analysis is a valuable tool for understanding the behavior of antennas and ensuring that they are designed for optimal performance. Micro-strip antennas represent a promising candidate in radio-communication systems because of their reduced cost, light weight and good performance. However, the small bandwidth of these antennas frequently restricts their range of use. By altering the radiating patch geometry using the etching technique, enhancing the impedance bandwidth of this kind of antenna becomes possible. In this paper, an original patch antenna is designed and investigated. The design of this latter is carried out using two rectangular slots together with a reduced-size ground plane in order to extend the UWB operating spectrum while keeping a low return loss. The analysis of the studied antenna performance is conducted utilizing the theory of characteristic modes, which is based on eigenvalues and eigen-current representation. The following sections provide a study of the design process and a discussion of the measured results.

2. THEORY OF CHARACTERISTIC MODES

The characteristic mode is the orthogonal current mode on an equipotential surface. CMA is a method for calculating the current-distribution modes of any conductor in a perfect vacuum with no feed port. Modal significance, eigenvalues, characteristic angle, field radiation and surface current give a global insight into various resonances and modes in order to determine the dominant resonating modes of a specific antenna.

The antenna current distribution overlaps in various modes in CMT applications and each mode is featured by the modal weighting coefficient (distinctive angle α_n) and the radiation efficiency that the eigenvalue (λ_n) indicates. The real current density J on the antenna equipotential surface, as according to CMT, is written as a rectilinear combination of characteristic mode currents J_n :

$$J = \sum_n (J_n \alpha_n) \quad (1)$$

The eigenvalue (λ_n) describes the proportion of reactive power to radiative power. If $\lambda_n = 0$, the mode radiates well at this frequency. The characteristic current distribution modes are determined from the generalized eigenvalue formula, which is given as:

$$X(J_n) = \lambda_n R(J_n) \quad (2)$$

where R and X stand for the real and imaginary parts of the generalized impedance operator $Z = R + jX$ and J_n represents the characteristic currents or eigenvectors which are solutions of the global eigenvalue formula. When the value of λ_n takes a very high value vs. the frequency plot, the eigenvalues cannot be used to categorize the dominant mode of the antenna. The characteristic angle (α_n) can be used to tackle this problem, which is given by the subsequent expression:

$$\alpha_n = 180 - \tan^{-1}(\lambda_n) \quad (3)$$

Each mode contribution to the overall electromagnetic reaction to a certain source is measured by the modal significance (MS_n), which is defined by the subsequent expression:

$$MS_n = \left| \frac{1}{1 + j\lambda_n} \right| \quad (4)$$

The resonance point of MS typically has a value of one "1," while the modes that do not contribute to the

resonance have a value of zero "0." and the characteristic angle (α_n) has a 180° phase difference for the resonating mode; therefore, λ_n is equal to zero.

3. CHARACTERISTIC MODE PERFORMANCE ANALYSIS

In this part, we analyze the performance of a broadband antenna using the theory of characteristic modes. Knowing that the notion of characteristic mode is based on the study of the radiating element without a structure, it is simply dependent on the size and form of the conducting item without the feeding port, in order to analyze and predict its electromagnetic behavior. This analysis allows for the computation of the antenna electrical properties, such as its resonant frequency and impedance, without the need for a physical structure to be built. This can save time and resources, as well as provide insight into the optimal design for the antenna. This analysis can also be used to identify potential issues with the design and optimize the antenna for specific performance objectives. The eigenvalue gives insight into the nature of the mode. If $\lambda_n=0$, it means that the mode has an effective radiation. The goal is to achieve the large-scale performance of the proposed antenna that can be achieved through various excitation modes in a simultaneous way. Here are the steps for analyzing antenna performance based on characteristic modes (CMs): The first step is to create the antenna model, choose the materials and determine the physical structure (shape and size) of the antenna. The second step is to identify and analyze the resonance modes, calculate the resonance patterns of the antenna to determine its characteristics and radiation pattern and evaluate the antenna performance (the first six modes were studied).

Finally, the modified antenna design is validated using simulations and experimental measurements to ensure that it meets the required performance criteria. These steps contributed to improving the design and choosing the appropriate shape and size. Figure 1 represents the eigenvalue for the first six modes. In fact, the selection of the first six modes in a characteristic mode analysis is typically based on practical considerations, such as computation time and accuracy. These first six modes provide a good approximation of the antenna behavior in most cases and are often sufficient for many design and analysis purposes. In general, using more modes in the characteristic mode analysis can provide results that are more accurate, but it also increases computation time and complexity. It is noted that the first six modes are often a trade-off between accuracy and computational efficiency. Additionally, in many cases, the higher-order modes may not significantly affect the overall behavior of the antenna, making the first six modes a sufficient representation of the antenna behavior. So, as we can see in Figure 1, the results clearly show that the six modes are resonant with ($\lambda_n = 0$). It is noted that the eigenvalues of the six modes contribute to dominant electromagnetic radiation strongly at their own frequencies. They offer resonances simultaneously at 5.83 GHz, 7.79 GHz, 10.1 GHz, 10.54 GHz, 12.75 GHz and 16.58 GHz. Also, a comprehension of the EM properties of the antenna could be possible from eigenvalues without taking the absorbed power and current into account.

Figure 2 displays the graph of the frequency of the first six modes *versus* the modal significance and characteristic angle. From Figure 2 (a), it is observed that mode-1, mode-2, mode-3, mode 4, mode-5 and mode-6 have large modal significance values around 1 at resonant frequencies of 5.83 GHz, 7.79 GHz, 10.1 GHz, 10.54 GHz, 12.75 GHz and 16.58 GHz, respectively. The ($\alpha_n = 180^\circ$) characteristic angle associated to these modes indicates that the antenna accumulates magnetic energy (inductive) when $\alpha_n < 180^\circ$ and when $\alpha_n > 180^\circ$, it accumulates electric charge (capacitive). As shown in Figure 2 (b), it is clear that modes (1, 2, 3, 4, 5 and 6) intersect the 180-degree axis line at 5.83 GHz, 7.79 GHz, 10.1GHz, 10.54 GHz, 12.75 GHz and 16.58 GHz, respectively.

Figure 3 shows the modes of surface currents and the 3-D farfield pattern for the six modes of the studied antenna at their respective resonance frequencies without a feed port. The current distribution over the ground plane and radiator produces a mix of successive pairs of even and odd modes from orthogonal currents. This simultaneous excitement of the odd and even modes provides the broadband radiation behaviour of a certain antenna. Also, it can be seen from farfield presentation that all CMs are varied with respect to the resonant frequency and that all modes emit radiation in all directions at their respective resonance frequencies.

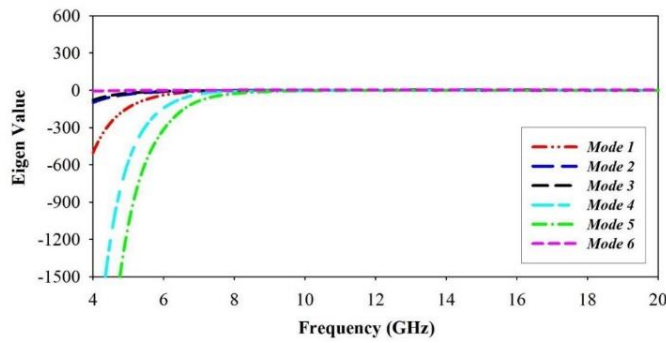


Figure 1. Eigenvalues as a function of frequency of the first six modes.

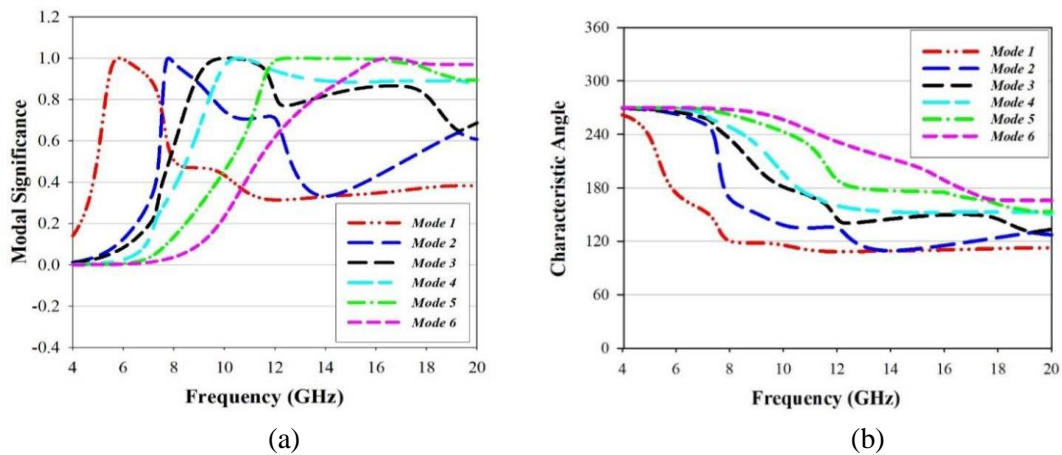


Figure 2. (a) Model significance, (b) Characteristic angle of the first six modes.

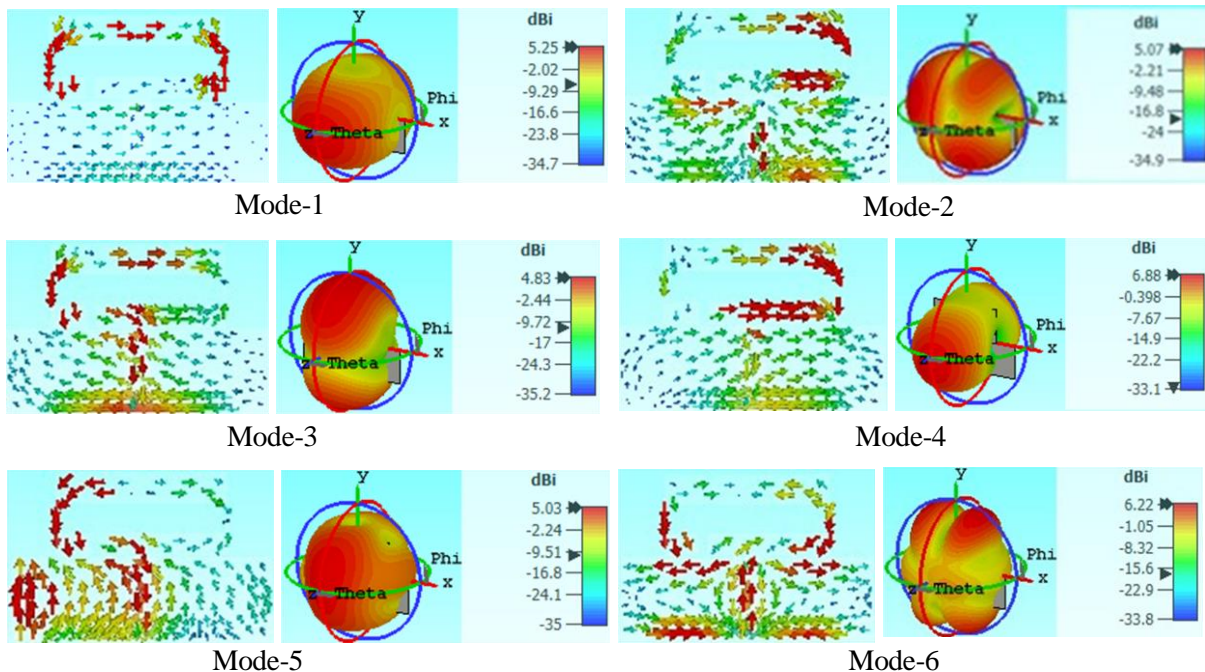


Figure 3. Surface current & 3-D farfield pattern at resonant CM frequencies.

4. ANTENNA DESIGN

In this section, the design process of the presented patch antenna is discussed. The antenna is mounted on a $28 \times 27 \times 1.6 \text{ mm}^3$ FR-4 substrate with a dielectric constant of 4.4 and a dielectric loss of 0.025, on which a 50Ω matched feedline with a length of $L_f = 9.2 \text{ mm}$ and a width of $W_f = 3.14 \text{ mm}$ is designed on the top face. Note that the reason behind the choice of the used laminate is its low profile characteristic. Figure 4 exhibits the final design of the proposed antenna.

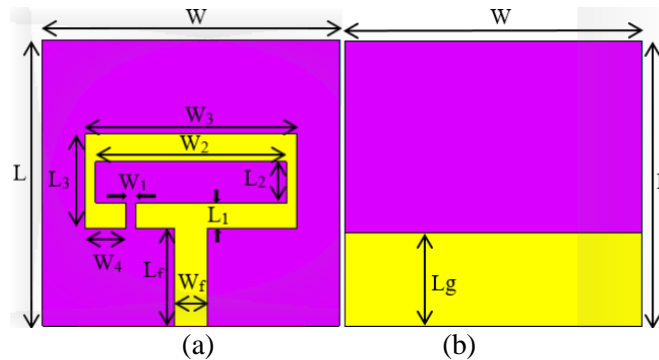


Figure 4. Final antenna geometry, (a) Front side, (b) Back side.

After a parametric study using CST Microwave Studio (MWS), the optimized parameters of the proposed UWB antenna are presented in Table 1.

Table 1. Final antenna dimensions.

Parameter	W	L	W_f	L_f	W_1	W_2	W_3	W_4	L_1	L_2	L_3	L_g	h
Value (mm)	28	27	3.1	9.2	1.	18	18.5	3.82	2.4	3.3	9	9	1.6

4.1 Design Evolution

As we can see from Figure 6, which depicts the simulated return loss at different steps of the presented antenna design, by utilizing a reduced ground plane in the second step, impedance matching has been enhanced at the lower and upper ranges of the operating spectrum, which has led to the manifestation of two resonant frequencies at 8 GHz and 18.5 GHz. Next, by moving to the third step that is based on forming a rectangular slot ($L_2 \times W_2$) on the radiating element, two resonant frequencies that correspond to 14.8 GHz and 17.5 GHz have been produced. Finally, by taking the fourth step, which is also based on employing one more rectangular open-ended slot ($L_1 \times W_1$) on the patch, three resonant frequencies have appeared at 6.2 GHz, 14.6 GHz and 17.2 GHz, with bandwidths of 1 GHz, 5.2 GHz and 3 GHz, respectively.

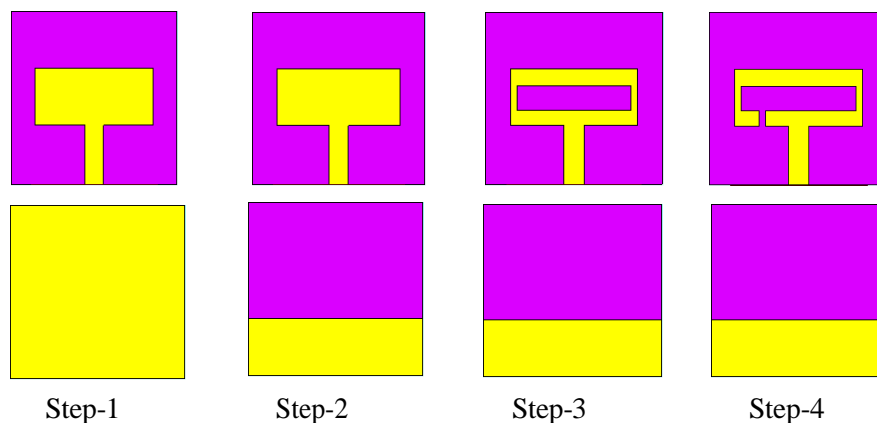


Figure 5. The proposed antenna design evolution.

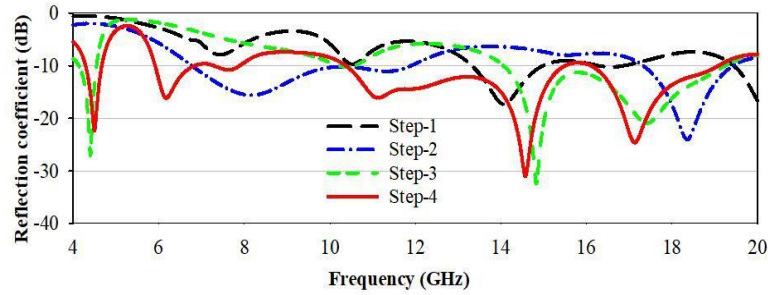


Figure 6. Simulated reflection coefficient for all different steps of the design.

4.2 Current Distribution

Figure 7 (a–d) shows the surface current of the presented antenna. It is obvious from this figure that the current propagates in all directions and is mainly concentrated at the feed point. Also, a significant amount of current is flowing around the edges of the openings $L_1 \times W_1$ and $L_2 \times W_2$, since the aperture acts as a slot that allows the electric field to penetrate into the antenna and create the surface current that flows around the edges of the aperture and generates the electromagnetic field necessary for radiation or reception. Finally, at higher frequencies, it is clear that the surface current is more concentrated near the edges of the antenna.

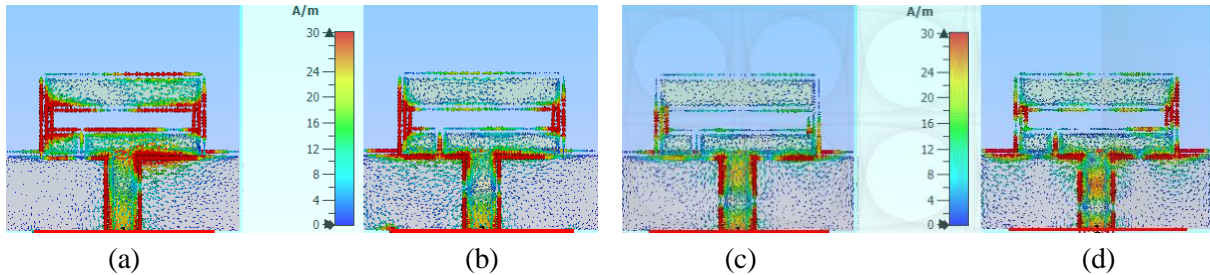


Figure 7. Current distribution at (a) 5.8 GHz, (b) 7.44 GHz, (c) 11 GHz and (d) 14.48 GHz.

5. PARAMETRIC STUDY

5.1 L_1 and L_2 Effect

Figure 8 shows the simulated reflection coefficients for different values of L_1 and L_2 . It is obvious that as L_1 decreases, the bandwidth decreases, noting that the optimal value of L_1 is 2.4 mm. Also, the rise in the L_2 value causes a decrease in the bandwidth, noting also that the optimal value of L_2 is 3.3 mm.

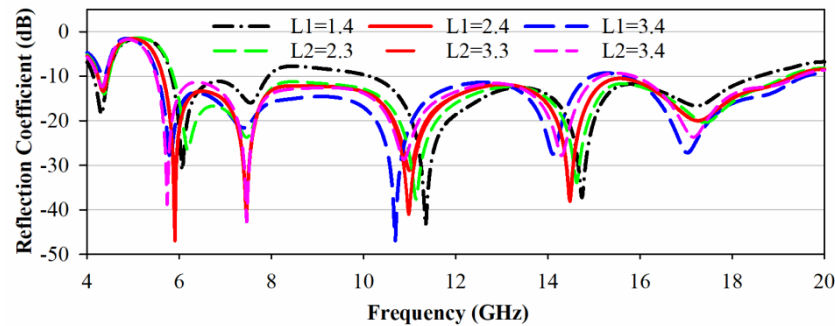


Figure 8. Simulated S_{11} with varying L_1 and L_2 .

5.2 W_1 and W_2 Effect

Figure 9 shows the simulation reflection coefficients for different values of W_1 and W_2 . It is clear that a

rise or decrease in W_1 produces a decrease in bandwidth, knowing that $W_1 = 1$ mm is the optimal value. On the other hand, the rise in the W_2 value causes a decrease in the bandwidth, knowing also that the optimum value of W_2 is 18 mm.

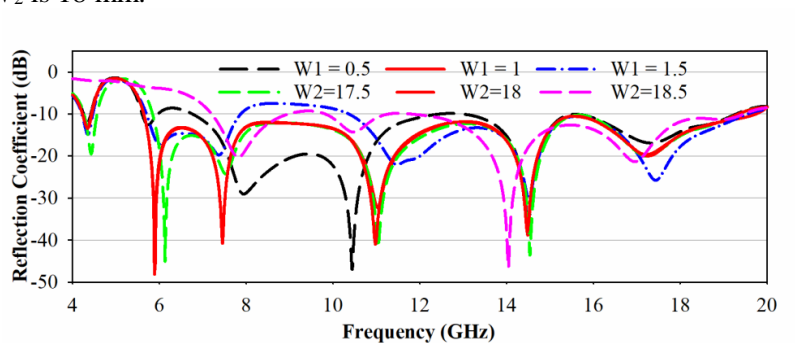


Figure 9. Simulated S_{11} with varying W_1 and W_2 .

5.3 Lg Effect

Figure 10 shows the simulation reflection coefficients for various values of L_g . The value of L_g was changed from 8 mm to 10 mm. It is clear that an increase or decrease in the value of L_g generates a decrease in bandwidth, noting that the optimum value for L_g is 9 mm.

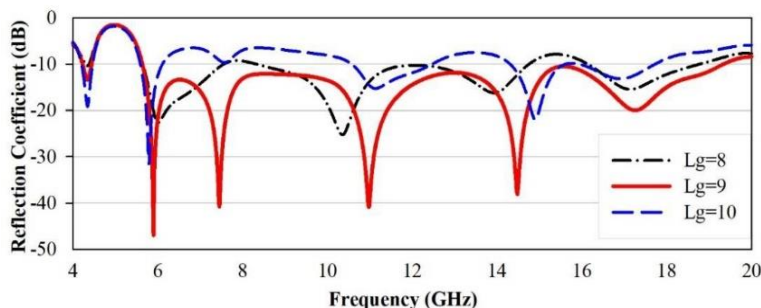


Figure 10. Simulated S_{11} with varying L_g .

6. SIMULATION RESULTS AND DISCUSSION

For experimental validation and according to the optimized dimensions specified in Table 1, a prototype of the suggested antenna has been fabricated on an FR-4 substrate using the circuit-board plotter LPKF Protomat (as seen in Figure 11), while the measurement was carried out utilizing the ZVB20 vector network analyzer. Figure 12 illustrates the simulated and measured s-parameter. The experimental results indicate that the proposed antenna provides a good impedance bandwidth that equals 13.8 GHz from 5.2 GHz to 19 GHz. Note that there is a good agreement between measured and simulated results, with the exception of a slight difference caused by the lossy nature of the used laminate FR-4, SMA connections and soldering.

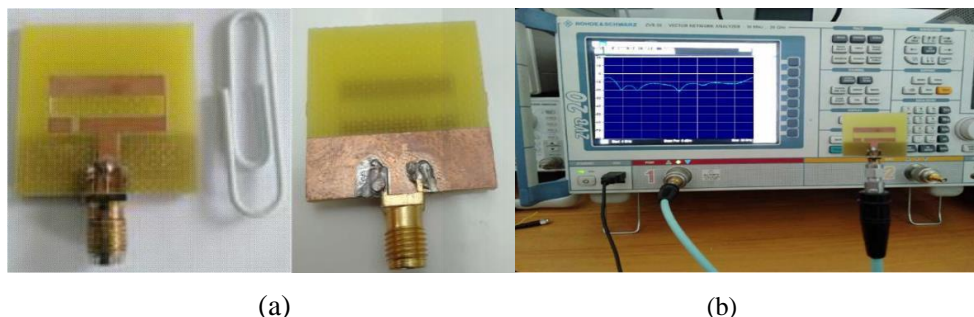


Figure 11. (a) Front and back view of the fabricated antenna, (b) measurement setup.

6.1 Gain

The measured and simulated gain and efficiency are shown in Figure 13. As we can see from this figure, this antenna provides a good gain that ranges from 3.55 dBi to 6.3 dBi, noting that its maximum gain is attained at 9.6 GHz. Additionally, we can say that this antenna is highly efficient, since it has attained a maximum efficiency of about 86.8 % at 9 GHz while maintaining an efficiency of at least 73.8 % over all the frequency band of interest.

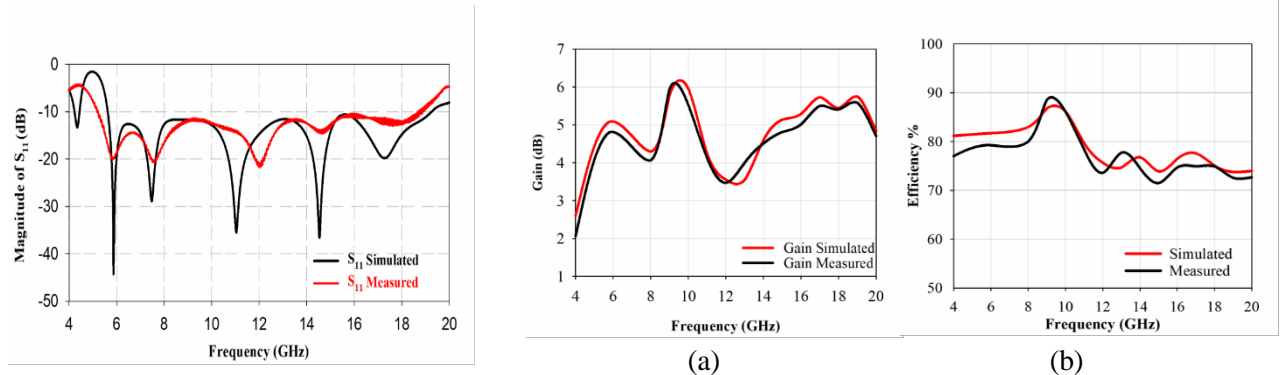


Figure 12. Measured and simulated magnitude of S_{11} .

Figure 13. The measured and simulated (a) peak gain, (b) efficiency.

6.2 Farfield Pattern

The measured and simulated E-plane and H-plane radiation patterns are depicted in Figure 14 (a–d), respectively. Due to the large bandwidth, only four frequencies are presented: 5.8 GHz, 7.44 GHz, 11 GHz and 14.48 GHz. So, from these diagrams, it can be seen that the proposed antenna is characterized by a quasi-omnidirectional radiation pattern in the H-plane. The radiation behavior of the antenna presented in the E-plane is similar to that of a dipole. Note that at 14.48 GHz, the 2D farfield patterns are less omnidirectional because of the higher-order resonances. Figure 15 displays the Geozondas antenna measurement system that was utilized. In order to determine the antenna radiation pattern, a horn antenna was utilized as the transmitting antenna and the receiving antenna was the antenna being tested.

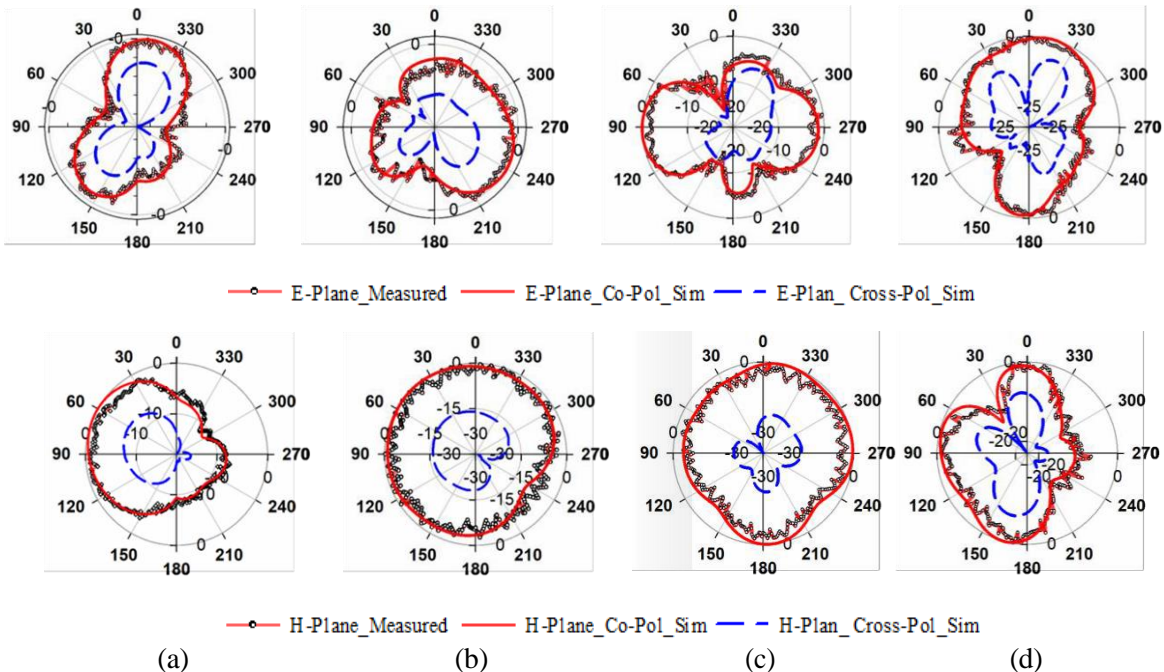


Figure 14. Measured and simulated E-plane & H-plane farfield patterns at (a) 5.8 GHz, (b) 7.44 GHz, (c) 11 GHz and (d) 14.48 GHz.

7. COMPARISON

Table 2 illustrates the performance comparison of the presented antenna with those of antennas presented in recently reported works based on bandwidth, gain, size and efficiency. Based on this comparison, it is clear that the studied UWB antenna is characterized by its small size, high gain, high efficiency and wide impedance bandwidth compared to those introduced in other works, which proves the presented antenna efficiency.

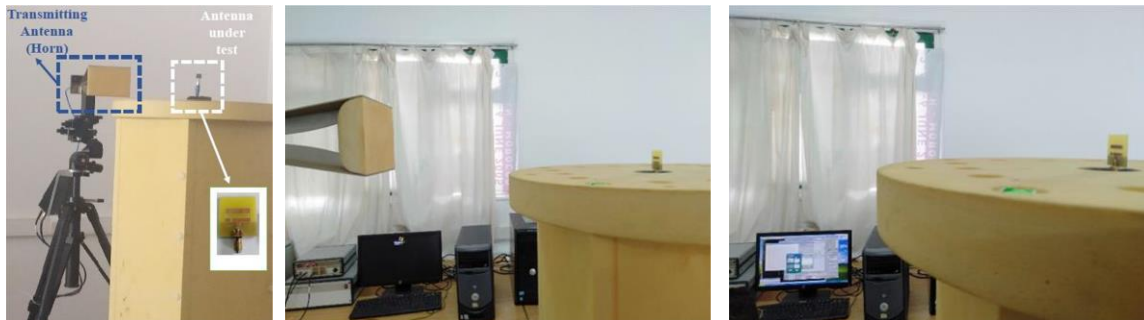


Figure 15. The proposed antenna measurement setup.

Table 2. Comparison between the proposed work and earlier works.

Ref.	Freq. Band	Gain (dBi)	Overall size (mm ³) (λ^3)	Efficiency (%)	Operating band (GHz)
[13]	9.4	3.8– ~5.8	50×50×1.52 1.13 λ_0 ×1.13 λ_0 ×0.034 λ_0	88–98	(2.1–11.5)138%
[14]	12.1	4.85 max	32×32×1.6 0.95 λ_0 ×0.95 λ_0 ×0.048 λ_0	70–79.2	(2.9–15)135%
[15]	11.2	2.1–6.15	27 × 36 × 1.6 0.76 λ_0 ×1.01 λ_0 ×0.045 λ_0	---	(2.8-14)133%
[16]	2.59	-2–6.3	38.88 × 39.8 × 0.762 0.46 λ_0 ×0.47 λ_0 ×0.009 λ_0	---	(2.26 – 4.85)72%
[17]	2.36	5.26 max	97 × 76 × 0.7 1.33 λ_0 ×1.04 λ_0 ×0.010 λ_0	---	(2.94–5.3)57.3%
[18]	7.5	7 – 10	100 × 45 × 0.5 2.42 λ_0 ×1.09 λ_0 ×0.012 λ_0	---	(3.5 – 11)103%
[19]	2.6	4.64 max	30 ×30×0.8 0.39 λ_0 ×0.39 λ_0 ×0.010 λ_0	---	(2.61–5.21)66.5%
[20]	2.6	3.65 max	54 × 54 × 1.6 0.52 λ_0 ×0.52 λ_0 ×0.015 λ_0	---	(1.6 – 4.2)89.7%
[21]	4.22	5.32 max	50 × 50 × 1.6 0.76 λ_0 ×0.76 λ_0 ×0.024 λ_0	88.5	(2.48 – 6.7)91.9%
[22]	0.98	2.68 max	50 x 55x 1.6 0.43 λ_0 ×0.47 λ_0 ×0.014 λ_0	---	(2.08–3.06)38.1%
This work	13.7	3.55 – 6.3	27 x 28 x 1.6 1.12 λ_0 ×1.16 λ_0 ×0.066 λ_0	73.8–86.8	(5.64-19.34)109.7%

NOTE: Due to the absence of measurement results for certain antennas, all values are from simulation results. Calculation of the electrical volume has been carried out at the center of the bandwidth.

8. CONCLUSION

In this work, a compact broadband (UWB) antenna is studied and analyzed by applying the theory of characteristic modes (TCM). The results of the simulation and measurement showed good performance

of the broadband antenna behaviour of about 109.7% (5.64–19.34 GHz) and 114% (5.2–19 GHz), a high efficiency of about 86.8% and a maximum gain of 6.3 dBi. These results prove that this antenna is a great candidate for UWB applications and it can also be used in radio systems such as WLAN (5.15–5.90 GHz), ISM (5.725–6.875 GHz), mobile satellite applications (7.250–7.375 GHz), mobile applications (8.020–8.200 GHz), broadcasting satellites (12.4–12.5 GHz) and define systems (14.62–15.23 GHz).

ACKNOWLEDGEMENTS

The authors would like to thank Professor Alia ZAKRITI of ENSA, the National School of Applied Sciences, Abdelmalek Essaadi University, Tetuan, Morocco, for his support with regards to the fabrication of the proposed antenna.

REFERENCES

- [1] M. Windler and D. G. Camell, "Measuring Antennas above 1 GHz," Proc. of the 14th Intl. Electromagnetic Compatibility (EMC) Symposium, NIST, pp. 91–95, Feb. 2001.
- [2] M. Gupta and V. Mathur, "Wheel Shaped Modified Fractal Antenna Realization for Wireless Communications," AEU - Int. J. Electronics and Communications, vol. 79, pp. 257–266, Sep. 2017.
- [3] A. A. Deshmukh and P. V. Mohadikar, "Modified Rectangular Shape Patch Antennas for Ultra-wide Band and Notch Characteristics Response," Microwave and Optical Technol. Letters, vol. 59, no. 7, pp. 1524–1529, 2017.
- [4] A. Raza, W. Lin, Y. Chen et al., "Wideband Tapered Slot Antenna for Applications in Ground Penetrating Radar," Microwave and Optical Technol. Letters, vol. 62, no. 7, pp. 2562– 2568, 2020.
- [5] Y. Zehforoosh, M. Mohammadifar, A. Houshang Mohammadifar and S. R. Ebadzadeh, "Designing Four Notched Bands Microstrip Antenna for UWB Applications, Assessed by Analytic Hierarchy Process Method," J. Microwave, Optoelectronics and Electromagnetic Appl., vol. 16, no. 3, pp. 765–776, Sep. 2017.
- [6] H. Du, X. Yu, H. Zhang and P. Chen, "Design of Broadband and Dual-polarized Dielectric-filled Pyramidal Horn Antenna Based on Substrate-integrated Waveguide," Microwave and Optical Technology Letters, vol. 61, no. 3, pp. 702-708, 2019.
- [7] A. Chaabane and M. Guerroui, "Printed UWB Rhombus Shaped Antenna for GPR Applications," Iranian J. of Electrical and Electronics Eng., vol. 17, no. 4, pp. 2041–2041, Dec. 2021.
- [8] B. Bhandari, A. Kumar, T. Giri and D. Shah, "Design of CPW-fed Triangular Shaped UWB Antenna for Multiband Applications," Int. Research J. of Eng. and Tech. (IRJET), vol. 4, no. 7, pp. 2123-2128, Jul. 2017.
- [9] C.-J. Wu, I.-F. Chen, C.-M. Peng, W.-Y. Tsai and J.-S. Sun, "A Compact Fractal-shaped O-ring Monopole Antenna for Modern Broadband Wireless Applications," WSEAS Trans. Electron., vol. 12, pp. 93–99, 2021.
- [10] K. R. Xiang and F.C. Chen "A Method for Increasing the Bandwidth of Slot and Patch Antennas Using Grid-slotted Patch," Int. J. of RF Microwave Computer-aided Engineering, vol. 31, no. 2, p. e22510, 2021.
- [11] J.-Y. Deng et al., "Bandwidth and Gain Improvements of Low-profile H-shaped Microstrip Patch Antenna under Quadruple-mode Resonance," Int. J. RF Microw. Comp.-Aided Eng., vol. 30, no. 10, p. e22372, 2020.
- [12] N. M. Awad and M. K. Abdelazeez, "Multi-slot Micro-strip Antenna for Ultra-wide Band Applications," J. of King Saud Uni. - Engineering Sciences, vol. 30, no. 1, pp. 38–45, Jan. 2018.
- [13] P. M. Paul, K. Kandasamy, M. S. Sharawi and B. Majumder, "Dispersion-engineered Transmission Line Loaded Slot Antenna for UWB Applications," IEEE Antennas and Wireless Propagation Letters, vol. 18, no. 2, pp. 323–327, Feb. 2019.
- [14] S. Mohandoss et al., "Fractal Based Ultra-wideband Antenna Development for Wireless Personal Area Communication Applications," AEU-Int. J. Electronics and Communications, vol. 93, pp. 95–102, Sep. 2018.
- [15] H. S. Mewara et al., "A Printed Monopole Ellipsoid UWB Antenna with Four Band Rejection Characteristics," AEU-Int. J. Electronics and Communications, vol. 83, pp. 222– 232, Jan. 2018.
- [16] U. Ullah and S. Koziel, "A Novel Coplanar-strip-based Excitation Technique for Design of Broadband Circularly Polarization Antennas with Wide 3 dB Axial Ratio Beamwidth," IEEE Trans. on Antennas and Propagation, vol. 67, no. 6, pp. 4224–4229, Jun. 2019.
- [17] W. An, S. Li, W. Sun and Y. Li, "Low-profile Wideband Microstrip Antenna Based on Multiple Modes with Partial Apertures," IEEE Antennas and Wireless Propagation Letters, vol. 18, no. 7, pp. 1372- 1376, 2019.
- [18] Y. Sun and H. Jin, "Design of Broadband Endfire Antenna with Split-ring Resonator (SRR) Structures," Proc. of the 2019 IEEE Int. Conf. on Computational Electromagnetics (ICCEM), pp. 1–3, DOI: 10.1109/COMPEM.2019.8779224, Shanghai, China, Mar. 2019,
- [19] R. S. Daniel, "Broadband μ -negative Antenna Using ELC Unit Cell," AEU-Int. J. Electronics and Communications, vol. 118, p. 153147, May 2020.

- [20] M. Moore, Z. Iqbal and S. Lim, "A Size-reduced, Broadband, Bidirectional, Circularly Polarized Antenna for Potential Application in WLAN, WiMAX, 4G and 5G Frequency Bands," Progress In Electromagnetics Research C, vol. 114, pp. 1–11, Jan. 2021.
- [21] O. Benkhadda et al., "Compact Broadband Antenna with Vicsek Fractal Slots for WLAN and WiMAX Applications," Applied Sciences, vol. 12, no. 3, Article no. 3, Jan. 2022.
- [22] C. Güler, S. E. B. Keskin and R. B.aymaz, "The Development of Broadband Microstrip Patch Antenna for Wireless Applications," Bitlis Eren University J. of Science, vol. 11, no. 3, Article no. 3, Sep. 2022.
- [23] J. Budania, M. Sharma, R. Yadav and R. Dhara, "Characteristic Mode Analysis and Design of Broadband Circularly Polarized CPW-fed Compact Printed Square Slot Antenna," Progress in Electromagnetics Research M, vol. 94, pp. 105-118, 2020.
- [24] R. Harrington and J. Mautz, "Theory of Characteristic Modes for Conducting Bodies," IEEE Trans. on Antennas and Propagation, vol. 19, no. 5, pp. 622–628, Sep. 1971.
- [25] Y. Chang and R. Harrington, "A Surface Formulation for Characteristic Modes of Material Bodies," IEEE Trans. on Antennas and Propagation, vol. 25, no. 6, pp. 789–795, Nov. 1977.
- [26] R. F. Harrington and J. R. Mautz, "Characteristic Modes for Aperture Problems," IEEE Trans. on Microwave Theory and Techniques, vol. 33, no. 6, pp. 500–505, Jun. 1985.
- [27] M. Cabedo-Fabres, E. Antonino-Daviu, A. Valero-Nogueira and M. F. Bataller, "The Theory of Characteristic Modes Revisited: A Contribution to the Design of Antennas for Modern Applications," IEEE Antennas and Propagation Magazine, vol. 49, no. 5, pp. 52–68, Oct. 2007.
- [28] Y. Wu, H. Lin, J. Xiong, J. Hou, R. Zhou, F. Deng and R. Tang, "A Broadband Metamaterial Absorber Design Using Characteristic Modes Analysis," Journal of Applied Physics, vol. 129, no. 13, p. 134902, 2021.
- [29] F. H. Lin and Z. N. Chen, "Low-profile Wideband Metasurface Antennas Using Characteristic Mode Analysis," IEEE Transactions on Antennas and Propagation, vol. 65, no. 4, pp. 1706-1713, 2017.
- [30] T. Li and Z. N. Chen, "Wideband Sidelobe-level Reduced Ka-Band Metasurface Antenna Array Fed by Substrate-integrated Gap Waveguide Using Characteristic Mode Analysis," IEEE Transactions on Antennas and Propagation, vol. 68, no. 3, pp. 1356-1365, 2020.

ملخص البحث:

تمّ تصميم هوائي صغير الحجم عريض النطاق أبعاده $27\text{م} \times 28\text{م} \times 1.6\text{م}$ وله مواعمة ممانعة جيدة للأنظمة الراديوية عريضة النطاق ذات المدى القصير. ولتحسين مواعمة الممانعة، تمّ إنشاء شقين مستطيلين على عنصر الإشعاع مع تصغير الحجم في المستوى الأرضي من أجل توسيع النطاق الترددي فائق العرض للهوائي. وقد جرى تحليل عرض النطاق والأداء الإشعاعي للهوائي باستخدام نظرية الأنماط المميّزة (TCM).

تمّت مقارنة أداء الهوائي بالموصفات المرغوبة وكذلك تعديل الشكل والحجم لإنتاج إشعاع فعال ونمط إشعاع سائد. وكشفت النتائج أن الأنماط السّنة كانت في حالة رنين. وهذا يتضمّن أن القيم الذاتية للأنماط السّنة تسهم بقوة في الإشعاع الكهرومغناطيسي السائد وأنها تمتلك قيم أهمية تقارب (1) عند ترددات الرنين الخاصة بها. علاوة على ذلك، تبين من الزاوية المميّزة أنّ الهوائي في حالة رنين عند (180) درجة؛ لأنّ الأنماط السّنة تقطع خطّ المحور عند 180 درجة عند ترددات الرنين الخاصة بها. وتبين النتائج التجريبية نطاقاً عرضيه (109.7%) بين (5.64) جيجاهيرتز و (19.34) جيجاهيرتز، كما بينت أنّ الكسب الأعلى للهوائي بلغ (6.3) ديسيبل، بفاعلية اقتربت من (86.5%). وهذه النتائج تجعل من الهوائي الذي تمّ دراسته في هذا البحث خياراً فعالاً لتشكيلية واسعة من تطبيقات الاتصالات والتطبيقات الإلكترونية، علاوة على أنه سهل التركيب في الأماكن الضيقة بفعل خصائصه التصميمية البسيطة وحجمه الصغير ووزنه الخفيف.

